In: The Prion Phenomena in Neurodegenerative Diseases ISBN: 978-1-63483-399-8
Editors: Giuseppe Legname and Gabriele Giachin

Chapter 2

X-RAY FIBER DIFFRACTION FROM PRIONS: OF MICE AND BETA-SOLENOIDS

Holger Wille*

Centre for Prions and Protein Folding Diseases and Department of Biochemistry, University of Alberta, Edmonton, Alberta, Canada

ABSTRACT

Only limited information is available about the structure of the infectious prion protein, PrP^{Sc}, and of its proteolytically truncated homolog, PrP 27-30. Their insolubility and propensity to aggregate have frustrated all attempts to determine their structures by conventional approaches such as X-ray crystallography and solution NMR spectroscopy. X-ray fiber diffraction, however, has been used to analyze the structures of PrP^{Sc} and PrP 27-30 amyloid fibrils purified from the brains of infected laboratory rodents. The structures of eight rodent-adapted natural isolates and seven "synthetic" prion strains that originated *in vitro* were analyzed. The diffraction patterns from all brain-derived prion strains exhibited the same repeating unit of 19.2 Å, represented by a series of meridional diffraction signals at 4.8, 6.4, and 9.6 Å. The underlying structure, which appears to form the general architecture for the infectious mammalian prion, was identified as a four-stranded ß-solenoid in a cross-ß arrangement. In contrast, recombinant prion protein that was fibrillized *in vitro* was found to posses a different structure altogether, with a repeating unit of 4.8 Å per molecule and a characteristic equatorial diffraction signal at ~ 10 Å, indicative of stacked ß-sheets. A variety of shortened prion protein constructs and peptides were found to adopt structures of a reduced complexity, often in a stacked ß-sheet configuration. Therefore, studies to investigate the structure of the infectious mammalian prion cannot rely on more convenient surrogates.

* Corresponding Author address. Email: wille@ualberta.ca.

INTRODUCTION

Prions are responsible for a variety of neurodegenerative diseases in humans, agriculturally important livestock, and wild cervids. These diseases, which are invariably fatal, include Creutzfeldt-Jakob disease (CJD) in humans, bovine spongiform encephalopathy (BSE) in cattle, chronic wasting diseases (CWD) in deer, elk, and moose, as well as sheep and goat scrapie [1]. The mammalian prion protein (PrP) was found to undergo a profound structural change in its conversion from the benign, cellular isoform (PrP^{C}) to the disease-causing, infectious conformer (PrP^{Sc}) [2, 3]. The structure of PrP^{C} is reasonably well known through studies of recombinantly expressed PrP (recPrP) by solution NMR spectroscopy and X-ray crystallography [4]. In contrast, the structure of PrP^{Sc} is poorly understood owing to its propensity to aggregate and its general insolubility [5]. Numerous analytical techniques such as Fourier-transform infrared (FTIR) and circular dichroism (CD) spectroscopies, electron microscopy and electron crystallography, as well as mass spectrometry in concert with limited proteolysis, surface reactivity, and H/D exchange studies have been used to investigate the structure of PrP^{Sc} [6]. The conclusions drawn from these diverse experimental approaches have been limited by the inherent difficulties of working with an aggregated and insoluble protein.

In this chapter, I am summarizing the results of a series of studies on the structure of PrP^{Sc} and its N-terminal truncated variant PrP 27-30, using X-ray fiber diffraction [7, 8]. These studies spanned well over a decade and involved fruitful collaborations with many scientists, particularly Gerald Stubbs and his team at Vanderbilt University were indispensable for the success of the experiments. These long-term efforts were rewarded by unique insights into the fold of the infectious conformer. X-ray fiber diffraction, as a technique, gained fame by providing the experimental data that led to the discovery of the structure of DNA [9, 10] and has also been used to determine the structure of complex assemblies such as intact tobacco mosaic virus (TMV) [11].

PrP^{Sc} and PrP 27-30 are prone to aggregate into a variety of different quaternary structures such as amorphous aggregates, two-dimensional crystals, and amyloid fibrils [12]. Prominent among those structures are the amyloid fibrils, from which, because of their regular and repeating structure, detailed structural information about their underlying molecular architecture can be extracted. X-ray fiber diffraction takes advantage of the repeating nature of the protein subunits that make up the amyloid fibrils, and thus provides unique insights into the molecular architecture of the infectious conformer in its native state.

In order to collect useful X-ray fiber diffraction data from our experiments with PrP^{Sc} and PrP 27-30 we tried a variety of sample preparation techniques, but discovered that an approach similar to the one that was used to determine the structure of DNA gave the best results. We prepared dried fibers from suspensions of both PrP^{Sc} and PrP 27-30 amyloid fibrils. The dried fibers were made in microchambers fashioned from standard microcuvettes that are commonly used for spectroscopy [13]. The microchambers allowed the humidity of the sample to be controlled using concentrated salt solutions as desiccants in a closed environment (Figure 1). The humidity control proved to be essential to maintain a biologically relevant conformation, as had been demonstrated through X-ray fiber diffraction analyses of both Sup35 amyloid fibrils [13, 14] and fungal HET-s prions [15]. In fully dried samples the structures had collapsed into degenerate stacked β-sheet amyloids, while the

humidity controlled samples retained their native structure (a β-solenoid in case of the fungal HET-s prion [16]).

PrP^{Sc} AND N-TERMINALLY TRUNCATED PrP 27-30

Samples of full-length PrP^{Sc} and PrP 27-30 were purified from the brains of Syrian hamsters, wild type mice, and transgenic mice (overexpressing PrP from other species) that were infected with prions from one of several rodent-adapted natural isolates. These prion strains showed a wide range of properties, for example the level to which the diseased brain contains pre-formed amyloid fibrils: RML prions in FVB mice are devoid of amyloid fibrils, [17, 18] while Sc237 prions in SHa have widespread amyloid plaques throughout their brain [19]. The purification of these diverse prion strains was based on the repeated precipitation with phosphotungstate anions (PTA), [20] which by itself induces amyloid formation *in vitro* with both PrP^{Sc} and PrP 27-30 [18]. The latter fact proved to be very useful for our X-ray fiber diffraction experiments and contributed to the overall quality and quantity of the purified PrP^{Sc} and PrP 27-30 amyloids [8].

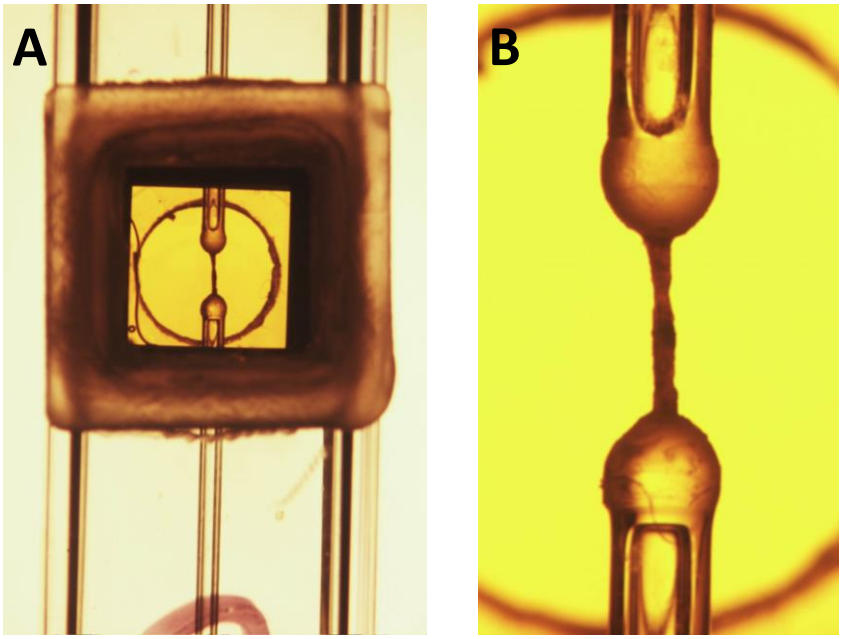

Figure 1. A dried fiber specimen of Syrian hamster (SHa) Sc237 PrP 27-30 in a humidity-controlled microchamber. (A) Low-power view of a microchamber with a single silicon-nitride window attached [13]. The silicon-nitride windows create a hermetic seal, while permitting the X-rays to reach the sample without undue scattering of the X-ray beam. Prior to the data collection at the synchrotron beamline, a lead-tape with a 5 mm pinhole to reduce unspecific X-ray scatter is attached (not shown). (B) High-power view of a dried SHa Sc237 PrP 27-30 fiber. The distance between the capped glass capillaries (top and bottom) is ~1.5 mm. While the fiber looks somewhat uneven, it did provide a fairly well-ordered diffraction pattern (comparable to Figure 2A).

The first X-ray fiber diffraction studies on PrP 27-30 were limited by the use of low intensity X-ray sources and the high degree of disorder in the prion samples [21]. In those diffraction patterns it was difficult to discern even the 4.8 Å diffraction on the meridian, which is a defining characteristic for the cross-β structure of amyloid [22]. Thus, no structural information was obtained at that time.

By using synchrotron-based X-ray sources (beamlines at the Stanford Synchrotron Radiation Laboratory (SSRL) and the Advanced Photon Source (APS)), which provide much higher intensity X-ray beams with a narrower collimation, we were able to collect diffraction patterns with unprecedented levels of information on the structure of prions. In addition, the use of PTA-purified prion preparations contributed significantly to the improved diffraction data [7]. The diffraction patterns from Syrian hamster PrP 27-30 revealed an axial repeating unit of 19.2 Å per molecule, represented by a series of meridional diffraction intensities at 4.8, 6.4, and 9.6 Å, respectively (Figure 2A, red arrows). This result indicated that the height of each molecule of PrP 27-30 is equivalent to four β-strands. The diffraction on the equator originated predominantly from lipid and detergent molecules (Figure 2A, black arrows), which co-purified with the prions or were added during the purification (as is the case with the detergent Sarkosyl). The absence of a strong ~10 Å equatorial diffraction, which is commonly seen with stacked β-sheet amyloids (compare Figure 2B), implied the presence of a β-helical or β-solenoidal structure instead [7].

Prior to our study, an X-ray fiber diffraction pattern from a β-helical or β-solenoidal amyloid had not been observed experimentally, and our interpretation of the PrP 27-30 diffraction data was the first time this particular fold had been suggested by this technique [7]. Fortuitously, around that time the structure of the fungal HET-s prion had been determined by solid-state NMR spectroscopy and was found to contain a two-rung β-solenoid [16, 23]. This structural similarity and the relative simplicity of expressing and refolding this non-pathogenic protein made it a good candidate for X-ray fiber diffraction studies. Right away it became apparent that the diffraction patterns of the β-solenoidal HET-s prion fibrils matched our prediction: The meridian revealed diffraction intensities at 4.8 and 9.6 Å (Figure 2C red horizontal arrows), respectively, indicating a two-stranded β-structure [24]. Furthermore, the equator was dominated by a series of intensities at 17 Å and 11 Å (Figure 2C red vertical arrows) typical of patterns whose structures approximate that of a solid cylinder such as a β-solenoid. A *dominant* ~10 Å equatorial diffraction, which is characteristic for stacked β-sheet amyloids, was notably absent.

The initial X-ray fiber diffraction studies were limited by using only two rodent-adapted scrapie strains: RML and Sc237 [7]. In order to extend the analyses to other prion strains, we purified PrP^{Sc} and PrP 27-30 from the brains of prion-infected Syrian hamsters, wildtype mice, and transgenic mice expressing sheep or elk PrP that were infected with a variety of rodent-adapted prion strains (Table 1). In detail, we examined four sheep or goat scrapie strains (Sc237, RML, 139H, and SSBP1), two transmissible mink encephalopathy (TME) strains (hyper and drowsy), and one isolate of bovine spongiform encephalopathy (301V) and chronic wasting disease each. Furthermore, we also included prions isolated from a transgenic mouse line expressing a P101L mutated version of PrP [25], which is analogous to the Gerstmann-Sträussler-Scheinker syndrome (GSS) mutation of P102L in human PrP [26].

With all of these prion strains we obtained nearly identical diffraction results (Table 1) indicating the presence of a four-rung β-helical or β-solenoid architecture, based on three

orders of diffraction (9.6 Å, 6.4 Å, and 4.8 Å) of a 19.2-Å repeating unit in each case [8]. This also included the spontaneously arising prions from the P101L GSS mimic.

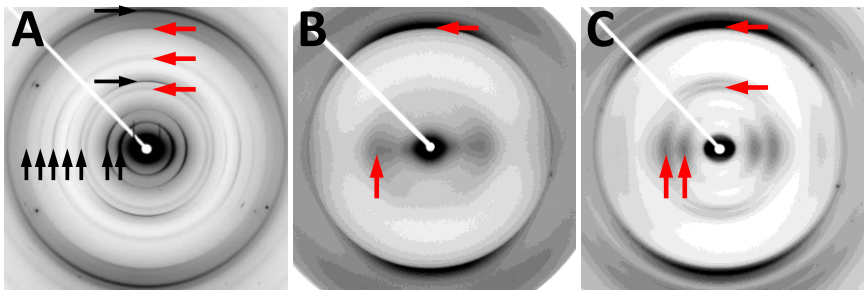

Figure 2. Comparison of X-ray fiber diffraction patterns from a rodent-adapted prion isolate, a recombinant PrP amyloid, and recombinant HET-s(218-289) amyloid. (A) Purified SHa Sc237 PrP 27-30 was used to produce a fairly well-ordered dried fiber (comparable to Figure 1B). The diffraction pattern contains signals originating from protein (red arrows) and lipid / detergent components (black arrows). Red arrows indicate meridional diffraction at close to 4.8, 6.4, and 9.6 Å (top to bottom), which correspond to the fourth, third, and second order diffraction of a 19.2 Å repeating unit. The lipid diffraction is dominated by meridional signals at 4.2 and 8.4 Å (black horizontal arrows), which stem from partially oriented lipids presumably associated with the glycosyl-phosphatidyl inositol (GPI) anchor of PrP. Lipid / detergent assemblies are responsible for a series of equatorial diffraction signals (black vertical arrows). The relatively high orders and sharpness of these intensities, as well as their spacings are characteristic of crystalline order [7]. (B) Diffraction pattern from recombinant murine PrP(89-230) amyloid that was fibrillized *in vitro*. The diffraction is dominated by meridional intensity at 4.8 Å (red horizontal arrow) and equatorial intensity close to 10 Å (red vertical arrow), typical of a stacked β-sheet amyloid [7, 24]. (C) Diffraction pattern from recombinant HET-s(218-289) amyloid fibrillized at pH 7. The structure of HET-s(218-289) amyloid had been determined by solid-state NMR spectroscopy to contain a two-rung β-solenoid structure [16, 23]. The meridional diffraction at 4.8 and 9.6 Å (red horizontal arrows, top to bottom) confirm the two-rung β-sheet conformation, while the equatorial diffraction at 11 and 17 Å (red vertical arrows, left to right) indicate the β-solenoid nature of this amyloid [24].

Table 1. X-ray fiber diffraction from rodent-adapted prion strains

Prion Strain	Disease of origin	Host species	β-sheet architecture
Sc237	Scrapie	Syrian hamster	4-rung β-solenoid[c]
139H	Scrapie	Syrian hamster	4-rung β-solenoid[c]
RML	Scrapie	mouse (FVB)	4-rung β-solenoid[a]
SSBP1	Scrapie	Tg14880 (sheep PrP)	4-rung β-solenoid[a]
301V	Bovine spongiform encephalopathy (BSE)	mouse (FVB)	4-rung β-solenoid[a]
Drowsy	Transmissible mink encephalopathy (TME)	mouse (FVB)	4-rung β-solenoid[b]
Hyper	Transmissible mink encephalopathy (TME)	Syrian hamster	4-rung β-solenoid[a]
Elk CWD	Chronic wasting disease (CWD)	Tg12584 (elk PrP)	4-rung β-solenoid[a]
GSS mutation (P102L)	Gerstmann-Sträussler-Scheinker syndrome (GSS)	Tg464 (mouse PrP: P101L)	4-rung β-solenoid[a]

Structure observed with [a] PrP^{Sc}, [b] PrP 27-30, and [c] PrP^{Sc} and PrP 27-30 preparations.
Data adapted from [8].

The general architecture for the structure of rodent-adapted prion isolates is shown in a cartoon depicting a four-rung β-helix or β-solenoid (Figure 3). At present, there is little evidence for structural elements beyond a β-helix or β-solenoid [6]. Therefore, the cartoon is limited to β-sheets in a roughly β-helical or β-solenoidal arrangement, no loops or other structural elements were included.

PRP PEPTIDES AND RECOMBINANT PRP AMYLOID

The difficulties that arise from working with infectious samples requiring biosafety level 2 conditions, such as the mammalian prions, limit the experimental techniques that can be employed. Furthermore, these difficulties also limit the researchers who can investigate these samples to those who have access to the appropriate facilities. To overcome this problem, synthetic peptides or short, recombinantly-expressed constructs of PrP are often used as surrogates for infectious specimens. While these models provide important insights into the behavior and folding properties of these surrogates, their relevance for the conformation of the biologically active, infectious prion is uncertain. This problem extends even to full-length recombinant PrP (recPrP(23-230)) and recombinant PrP(89-230) (recPrP(89-230)), which are often used to approximate PrP^{Sc} and PrP 27-30, respectively.

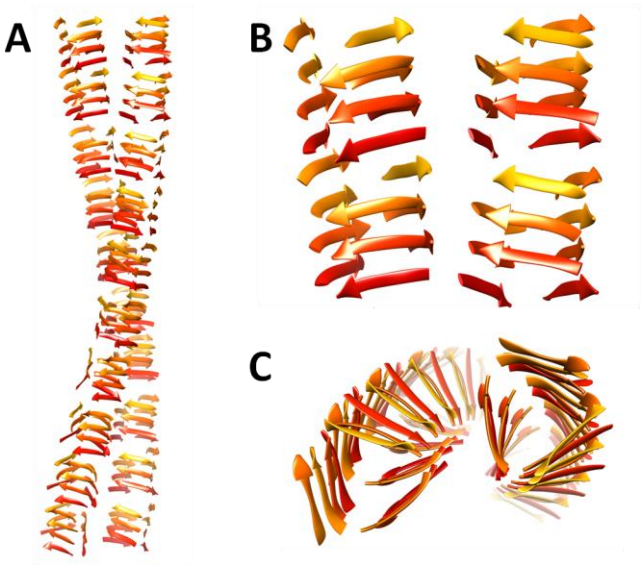

Figure 3. Cartoon graphic to illustrate the underlying structure that may give rise to the diffraction results obtained from brain-derived prion preparations. (A) Cartoon of two intertwined protein fibrils (protofilaments) consisting of individual molecules containing a four-rung parallel β-helix. (B) Detailed view of the top two molecules of the fibrils. In each case only the β-strands are depicted, loop and coil structures that would connect the individual β-strands are not shown. The four-rung β-helix has a height of 19.2 Å (= 4 x 4.8 Å). (C) View from the top of the fibrils illustrating two putative protofilaments.

In vitro generated amyloid from recPrP(23-230) and recPrP(89-230) conforms to the three hallmarks (compare [27]) that are required to use the term amyloid: 1) thin, unbranched protein fibrils, 2) which can be stained with Thioflavin T or Congo red dye, and which 3)

display the typical cross-β diffraction [22, 28]. Nevertheless, the X-ray fiber diffraction data clearly reveal that the *in vitro* generated amyloid preparations (Figure 2B) are structurally distinct from those of brain-derived prions (Figure 2A). The former are dominated by a very strong meridional diffraction at 4.8 Å and a strong equatorial diffraction at ~10 Å (Figure 2B), which are the characteristics of a stacked β-sheet structure [7, 29, 30].

In the next round of experiments we used X-ray fiber diffraction to explore the amyloidogenicity of different PrP peptides and constructs, and to assess to what degree they would be able to recapitulate the structural features of brain-derived prions. We fibrillized the respective substrates under a variety of conditions, which resulted in structural variations of the generated amyloid and complicated the interpretation to some degree [31]. In all cases, we were unable to produce amyloid with structural properties identical to those of brain-derived prions (Table 2). Nevertheless, in some cases the diffraction data indicated the presence of a β-helix or β-solenoid (PrP(89-143,P101L) and PrP(89-177)), but those peptides were restricted to only two rungs of β-structure by the length of the corresponding peptide. Therefore, these shorter versions of PrP are unable to accommodate a four-rung β-structure by design.

Table 2. X-ray fiber diffraction from PrP peptides and recombinant PrP amyloid

PrP construct	Size (amino acids) & species	Source	β-sheet architecture
PrP(106-126) [c]	21, human	synthetic peptide	stacked β-sheet
PrP(89-143,P101L) [c]	55, mouse	synthetic peptide	stacked β-sheet or 2-rung β-solenoid [a]
PrP(89-177) [c]	89, mouse, bank vole	recombinant protein	stacked β-sheet or 2-rung β-solenoid [a]
PrP(90-231) [b]	142, Syrian hamster	recombinant protein	stacked β-sheet
PrP(89-230) [b]	142, mouse	recombinant protein	stacked β-sheet
PrP(23-230) [d]	208, mouse	recombinant protein	stacked β-sheet

[a] Different structures observed under different conditions.
Data adapted from [b] [7]; [c] [31]; and [d] [8].

The PrP(23-144) peptide, which is based on the human Y145Stop mutation [32], was found to adopt a one-rung β-solenoid conformation [33]. While this study did not contain enough detail to determine the full structure of PrP(23-144) amyloid, it provided a good comparison to our data on the PrP(89-143,P101L) peptide [31]. In our hands the PrP(89-143,P101L) peptide was structurally pleiomorphic and capable of adopting both a stacked β-sheet and a two-rung β-solenoid (Table 2), which constitutes an acceptable agreement with the earlier investigation.

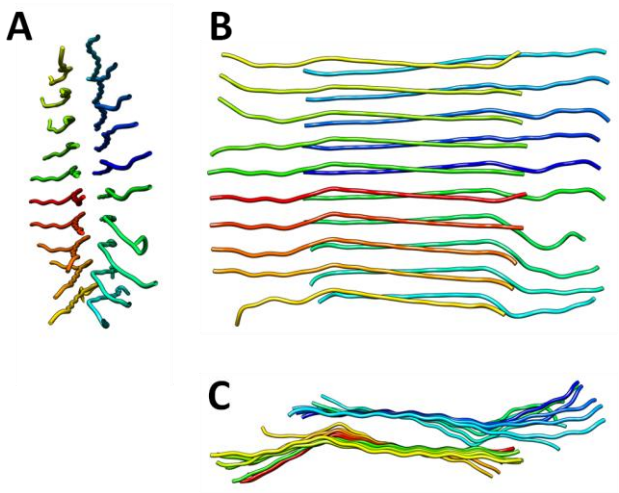

Figure 4. Graphic to illustrate the structure of a stacked β-sheet amyloid. The graphic is based on the PrP(106-126) peptide structure in its fibrillar state as determined by solid-state NMR spectroscopy [34]. (A, B) Two orthogonal side views of the stacked β-sheet amyloid structure of PrP(106-126). Each stack of molecules represents an independent β-sheet, formed through an in-register, parallel β-stacking of individual peptide molecules. The spacing between individual peptide strands in the β-sheet structure is 4.8 Å, which gives rise to a strong meridional diffraction signal at 4.8 Å. The β-sheet core of the amyloid structure is formed by the side-by-side association of two separate β-sheets (the overlapping region in B). (C) Top view of the fibril illustrating the ~10 Å spacing between neighboring β-sheets. This spacing is responsible for the 8-12 Å equatorial diffraction commonly seen with stacked β-sheet amyloid structures (compare Figure 2B). The PDB for this structure was kindly made available by Dr. Simon Sharpe (University of Toronto).

The structure of PrP(106-126) amyloid was determined by solid-state NMR spectroscopy [34], and is used here (Figure 4) to illustrate the general architecture of a stacked β-sheet amyloid. It is interesting to note that our X-ray fiber diffraction data from this peptide confirmed the general stacked β-sheet architecture, but that in our samples the peptide clearly formed a β-hairpin resulting in a molecular height of 9.6 Å [31]. Given the strength of the corresponding experimental data, this discrepancy cannot be attributed to experimental error, but instead re-emphasizes the structural pleiotropy of the prion protein and its truncated variants. This pleiotropy of the prion protein may also be a contributing factor to its ability to adopt distinct conformations such as those of PrP^{C} and PrP^{Sc}.

SYNTHETIC PRIONS

While recombinant PrP (recPrP) amyloid clearly differs structurally from brain-derived, infectious prions (Figure 2), various preparations of recPrP amyloid have given rise to “synthetic" prion strains upon inoculation into indicator animals [35, 36, 37, 38, 39, 40]. This apparent discrepancy between structure and (mal-)function was resolved by studying the structure of synthetic prions after repeated passage through transgenic mice (Table 3).

Table 3. X-ray fiber diffraction from rodent-passaged synthetic prion strains

Synthetic prion Strain	Original inoculum	Host species	β-sheet architecture
MoSP1	seeded recPrP amyloid	Tg9949 (mouse PrP)	4-rung β-solenoid [b]
MoSP2	unseeded recPrP amyloid	Tg9949 (mouse PrP)	4-rung β-solenoid [b]
MoSP5	seeded recPrP amyloid	Tg4053 (mouse PrP)	4-rung β-solenoid [a]
MoSP6	seeded recPrP amyloid	Tg4053 (mouse PrP)	4-rung β-solenoid [b]
MoSP7	seeded recPrP amyloid	Tg4053 (mouse PrP)	4-rung β-solenoid [b]
'rPrP-res'	PMCA with lipids & RNA	Tg4053 (mouse PrP)	4-rung β-solenoid [b]
SSLOW	unseeded recPrP amyloid	Tg7 (Syrian hamster PrP)	4-rung β-solenoid [b]

Structure observed with [a] PrP^{Sc} and [b] PrP 27-30.
Data adapted from [7, 8].

PrP^{Sc} and PrP 27-30 from different synthetic prion strains were purified from the brains of infected transgenic mice in an equivalent manner to the rodent-adapted natural isolates mentioned earlier (Table 1). The X-ray fiber diffraction data from all of the synthetic prion strains displayed the same three orders of meridional diffraction at 9.6 Å, 6.4 Å, and 4.8 Å, indicative of a 19.2 Å repeating unit as was seen earlier with rodent-adapted natural isolates [7, 8]. Furthermore, these samples also lacked a strong equatorial diffraction at ~10 Å indicative of a β-helical or β-solenoidal architecture. This finding places the synthetic prion strains into the same structural class as the natural prion isolates, supporting the interpretation that there may be only one infectious fold for the mammalian prion protein.

While the X-ray fiber diffraction data resolved the apparent structural discrepancy between synthetic prions and natural isolates, it raised another question: How can recPrP amyloids cause a prion infection, if it is has a different structure? One possible answer lies in the heterogeneity of the recPrP amyloid preparations that was observed with both the X-ray fiber diffraction experiments (Figure 2B) as well as negative stain electron microscopy (data not shown) [7, 8]. Thus, the bulk recPrP amyloid preparations with their predominantly stacked β-sheet conformation may have hidden a minor fraction of protein in the infectious β-helix or β-solenoid fold. This structural heterogeneity could easily explain the relatively low titers that were observed in most, if not all, initial transmissions [35, 36, 37, 38, 39, 40].

An alternative explanation suggested that inoculated recPrP amyloid may be subjected to deformed templating (heterogeneous seeding) *in vivo*, which may then give rise to the infectious β-helix or β-solenoid conformer [41, 42]. While the first option is difficult to exclude (and they are not necessarily mutually exclusive), the current experimental data favor the deformed templating hypothesis as the more influential alternative [41].

CONCLUSION

The data presented in this chapter indicate that all infectious mammalian prions share a common four-rung β-helix or β-solenoid architecture. These results are not in contradiction to prior efforts by other investigators to assign distinct structural features to the different prion strains (for example [20, 43, 44, 45]). Our findings merely indicate that this structural

diversity is based on a common four-rung β-helix or β-solenoid core. Thus the observed strain differences have to originate from more subtle structural differences.

The complex interplay between different levels of structure (secondary, tertiary, and quaternary structure), which define PrP^{Sc}, could explain the structural differences. For example, Aβ amyloid fibrils grown under quiescent or agitated conditions *in vitro*, showed clear differences in morphology and molecular architecture [46]. Electron paramagnetic resonance (EPR) spectroscopy demonstrated that morphological variations such as these could be based on relatively subtle differences in side-chain interactions between individual β-strands [47].

Moreover, the β-helix or β-solenoid fold has shown to provide sufficient variations to accommodate a wide range of molecular models for the structure of PrP^{Sc} [48, 49, 50, 51, 52, 53]. In all likelihood, none of the previously published models for the structure of PrP^{Sc} offer a realistic picture for the actual structure of the infectious prion [6]. Nevertheless, the β-helix or β-solenoid fold with its left- and right-handed variants represents a substantial territory of "fold-space," in which the structure of the infectious prion with all its strain variations can easily be accommodated. Together with the differences that can arise from subtle side-chain interactions alone [47], these alternatives provide enough structural variation to allow for distinct self-propagating prion folds, that is, strains.

ACKNOWLEDGMENTS

I would like to give special thanks to Gerald Stubbs for his advice and support in all matters X-ray fiber diffraction and his critical reading of the manuscript. Furthermore, I want to acknowledge Lillian Falese, Diane Latawiec, Ana Serban, Jan Stöhr, David W. Colby, Gültekin Tamgüney, Julian Ollesch, Alexander Borovinskiy, Amy Kendall, Michele McDonald, Wen Bian, and William Wan for their help in purifying the many prion samples and in collecting and analyzing the diffraction patterns. I am also indebted to Fred E. Cohen and Stanley B. Prusiner for their steadfast support for this project. Special thanks also belong to the beamline scientists at the Stanford Synchrotron Radiation Laboratory (SSRL) and the Advanced Photon Source (APS) for their support for the many data collection. Lastly, the experimental portions of this project were supported by grants from the National Institutes of Health (USA), the Fairchild Foundation, and the G. Harold and Leila Y. Mathers Foundation (to S.B.P., F.E.C., and G.S.). The writing of this chapter was backed by the Alberta Prion Research Institute (APRI) and the Helmholtz-Alberta Initiative on Neurodegenerative Disease Research (HAI-NDR).

REFERENCES

[1] Colby DW, Prusiner SB (2011) Prions. *Cold Spring Harb Perspect Biol* 3: a006833.

[2] Caughey BW, Dong A, Bhat KS, Ernst D, Hayes SF, et al. (1991) Secondary structure analysis of the scrapie-associated protein PrP 27-30 in water by infrared spectroscopy. *Biochemistry* 30: 7672-7680.

[3] Pan KM, Baldwin M, Nguyen J, Gasset M, Serban A, et al. (1993) Conversion of alpha-helices into beta-sheets features in the formation of the scrapie prion proteins. Proc Natl Acad Sci U S A 90: 10962-10966.

[4] Surewicz WK, Apostol MI (2011) Prion protein and its conformational conversion: a structural perspective. *Top Curr Chem 3*05: 135-167.

[5] Wille H, Prusiner SB (1999) Ultrastructural studies on scrapie prion protein crystals obtained from reverse micellar solutions. *Biophys J* 76: 1048-1062.

[6] Requena JR, Wille H (2014) The structure of the infectious prion protein: experimental data and molecular models. *Prion* 8: 60-66.

[7] Wille H, Bian W, McDonald M, Kendall A, Colby DW, et al. (2009) Natural and synthetic prion structure from X-ray fiber diffraction. *Proc Natl Acad Sci U S A* 106: 16990-16995.

[8] Wille H, Stöhr J, Bian W, Falese L, Tamgüney G, et al. (2015) *Manuscript in preparation.*

[9] Franklin RE, Gosling RG (1953) Molecular configuration in sodium thymonucleate. *Nature* 171: 740-741.

[10] Watson JD, Crick FH (1953) Molecular structure of nucleic acids; a structure for deoxyribose nucleic acid. *Nature* 171: 737-738.

[11] Namba K, Stubbs G (1986) Structure of tobacco mosaic virus at 3.6 A resolution: implications for assembly. *Science* 231: 1401-1406.

[12] Wille H, Shanmugam M, Murugesu M, Ollesch J, Stubbs G, et al. (2009) Surface charge of polyoxometalates modulates polymerization of the scrapie prion protein. *Proc Natl Acad Sci U S A* 106: 3740-3745.

[13] McDonald M, Kendall A, Tanaka M, Weissman JS, Stubbs G (2008) Enclosed chambers for humidity control and sample containment in fiber diffraction. *Journal of Applied Crystallography* 41: 206-209.

[14] Kishimoto A, Hasegawa K, Suzuki H, Taguchi H, Namba K, et al. (2004) beta-Helix is a likely core structure of yeast prion Sup35 amyloid fibers. *Biochemical and Biophysical Research Communications* 315: 739-745.

[15] Wan W, Stubbs G (2014) Fiber diffraction of the prion-forming domain HET-s(218-289) shows dehydration-induced deformation of a complex amyloid structure. *Biochemistry* 53: 2366-2370.

[16] Van Melckebeke H, Wasmer C, Lange A, Ab E, Loquet A, et al. (2010) Atomic-resolution three-dimensional structure of HET-s(218-289) amyloid fibrils by solid-state NMR spectroscopy. *J Am Chem Soc* 132: 13765-13775.

[17] Godsave SF, Wille H, Pierson J, Prusiner SB, Peters PJ (2013) Plasma membrane invaginations containing clusters of full-length PrPSc are an early form of prion-associated neuropathology in vivo. *Neurobiol Aging* 34: 1621-1631.

[18] Levine DJ, Stohr J, Falese LE, Ollesch J, Wille H, et al. (2015) Mechanism of Scrapie Prion Precipitation with Phosphotungstate Anions. *ACS Chem Biol* 10: 1269-1277.

[19] DeArmond SJ, McKinley MP, Barry RA, Braunfeld MB, McColloch JR, et al. (1985) Identification of prion amyloid filaments in scrapie-infected brain. *Cell* 41: 221-235.

[20] Safar J, Wille H, Itri V, Groth D, Serban H, et al. (1998) Eight prion strains have PrP(Sc) molecules with different conformations. *Nat Med* 4: 1157-1165.

[21] Nguyen JT, Inouye H, Baldwin MA, Fletterick RJ, Cohen FE, et al. (1995) X-ray diffraction of scrapie prion rods and PrP peptides. *J Mol Biol* 252: 412-422.

[22] Eanes ED, Glenner GG (1968) X-ray diffraction studies on amyloid filaments. *J Histochem Cytochem* 16: 673-677.

[23] Wasmer C, Lange A, Van Melckebeke H, Siemer AB, Riek R, et al. (2008) Amyloid fibrils of the HET-s(218-289) prion form a beta solenoid with a triangular hydrophobic core. *Science* 319: 1523-1526.

[24] Wan W, Wille H, Stohr J, Baxa U, Prusiner SB, et al. (2012) Degradation of fungal prion HET-s(218-289) induces formation of a generic amyloid fold. *Biophys J* 102: 2339-2344.

[25] Nazor KE, Kuhn F, Seward T, Green M, Zwald D, et al. (2005) Immunodetection of disease-associated mutant PrP, which accelerates disease in GSS transgenic mice. *EMBO J* 24: 2472-2480.

[26] Hsiao K, Baker HF, Crow TJ, Poulter M, Owen F, et al. (1989) Linkage of a prion protein missense variant to Gerstmann-Straussler syndrome. *Nature* 338: 342-345.

[27] Eisenberg D, Jucker M (2012) The amyloid state of proteins in human diseases. *Cell* 148: 1188-1203.

[28] Astbury WT, Dickinson S, Bailey K (1935) The X-ray interpretation of denaturation and the structure of the seed globulins. *Biochem J* 29: 2351-2360 2351.

[29] Jahn TR, Makin OS, Morris KL, Marshall KE, Tian P, et al. (2010) The common architecture of cross-beta amyloid. *J Mol Biol* 395: 717-727.

[30] Sunde M, Serpell LC, Bartlam M, Fraser PE, Pepys MB, et al. (1997) Common core structure of amyloid fibrils by synchrotron X-ray diffraction. *J Mol Biol* 273: 729-739.

[31] Wan W, Wille H, Stohr J, Kendall A, Bian W, et al. (2015) Structural Studies of Truncated Forms of the Prion Protein PrP. *Biophys J* 108: 1548-1554.

[32] Ghetti B, Piccardo P, Spillantini MG, Ichimiya Y, Porro M, et al. (1996) Vascular variant of prion protein cerebral amyloidosis with tau-positive neurofibrillary tangles: the phenotype of the stop codon 145 mutation in PRNP. *Proc Natl Acad Sci U S A* 93: 744-748.

[33] Skora L, Zweckstetter M (2012) Determination of amyloid core structure using chemical shifts. *Protein Science* 21: 1948-1953.

[34] Walsh P, Simonetti K, Sharpe S (2009) Core structure of amyloid fibrils formed by residues 106-126 of the human prion protein. *Structure* 17: 417-426.

[35] Colby DW, Giles K, Legname G, Wille H, Baskakov IV, et al. (2009) Design and construction of diverse mammalian prion strains. *Proc Natl Acad Sci U S A* 106: 20417-20422.

[36] Colby DW, Wain R, Baskakov IV, Legname G, Palmer CG, et al. (2010) Protease-sensitive synthetic prions. *PLoS Pathog* 6: e1000736.

[37] Deleault NR, Piro JR, Walsh DJ, Wang F, Ma J, et al. (2012) Isolation of phosphatidylethanolamine as a solitary cofactor for prion formation in the absence of nucleic acids. *Proc Natl Acad Sci U S A* 109: 8546-8551.

[38] Legname G, Baskakov IV, Nguyen HO, Riesner D, Cohen FE, et al. (2004) Synthetic mammalian prions. *Science* 305: 673-676.

[39] Makarava N, Kovacs GG, Bocharova O, Savtchenko R, Alexeeva I, et al. (2010) Recombinant prion protein induces a new transmissible prion disease in wild-type animals. *Acta Neuropathol* 119: 177-187.

[40] Wang F, Wang X, Yuan CG, Ma J (2010) Generating a prion with bacterially expressed recombinant prion protein. *Science* 327: 1132-1135.

[41] Makarava N, Kovacs GG, Savtchenko R, Alexeeva I, Budka H, et al. (2011) Genesis of mammalian prions: from non-infectious amyloid fibrils to a transmissible prion disease. *PLoS Pathog* 7: e1002419.

[42] Wan W, Bian W, McDonald M, Kijac A, Wemmer DE, et al. (2013) Heterogeneous seeding of a prion structure by a generic amyloid form of the fungal prion-forming domain HET-s(218-289). *J Biol Chem* 288: 29604-29612.

[43] Bessen RA, Marsh RF (1994) Distinct PrP properties suggest the molecular basis of strain variation in transmissible mink encephalopathy. *J Virol* 68: 7859-7868.

[44] Telling GC, Parchi P, DeArmond SJ, Cortelli P, Montagna P, et al. (1996) Evidence for the conformation of the pathologic isoform of the prion protein enciphering and propagating prion diversity. *Science* 274: 2079-2082.

[45] Peretz D, Scott MR, Groth D, Williamson RA, Burton DR, et al. (2001) Strain-specified relative conformational stability of the scrapie prion protein. *Protein Science* 10: 854-863.

[46] Petkova AT, Leapman RD, Guo Z, Yau WM, Mattson MP, et al. (2005) Self-propagating, molecular-level polymorphism in Alzheimer's beta-amyloid fibrils. *Science* 307: 262-265.

[47] Agopian A, Guo Z (2012) Structural origin of polymorphism of Alzheimer's amyloid beta-fibrils. *Biochem* J 447: 43-50.

[48] Wille H, Michelitsch MD, Guenebaut V, Supattapone S, Serban A, et al. (2002) Structural studies of the scrapie prion protein by electron crystallography. *Proc Natl Acad Sci U S A* 99: 3563-3568.

[49] Govaerts C, Wille H, Prusiner SB, Cohen FE (2004) Evidence for assembly of prions with left-handed beta-helices into trimers. *Proc Natl Acad Sci U S A* 101: 8342-8347.

[50] Stork M, Giese A, Kretzschmar HA, Tavan P (2005) Molecular dynamics simulations indicate a possible role of parallel beta-helices in seeded aggregation of poly-Gln. *Biophys J* 88: 2442-2451.

[51] Yang S, Levine H, Onuchic JN, Cox DL (2005) Structure of infectious prions: stabilization by domain swapping. *FASEB J* 19: 1778-1782.

[52] Kunes KC, Clark SC, Cox DL, Singh RR (2008) Left handed beta helix models for mammalian prion fibrils. *Prion* 2: 81-90.

[53] Shirai T, Saito M, Kobayashi A, Asano M, Hizume M, et al. (2014) Evaluating prion models based on comprehensive mutation data of mouse PrP. *Structure* 22: 560-571.